

# Full Potential Linearized Augmented Plane Wave Calculations of Structural and Optoelectronic Properties of $\text{KCdF}_3$

Madan Lal<sup>1</sup>, Shikha Kapila<sup>2</sup>

<sup>1</sup>Department of Physics, Govt Degree College Una, Himachal Pradesh-174303 (India)  
Research Scholar, I.K. Gujral Punjab Technical University, Jalandhar Punjab -144603 (India)

<sup>2</sup>Department of Applied Science, Bahra Group of Institutions, Bhedpura Patiala Punjab -147001 (India)

**Abstract:** A theoretical study of structural and optoelectronic properties of ternary oxides such as  $\text{KCdF}_3$  are investigated through the full potential linearized augmented plane wave (FP-LAPW) method in the density functional theory. The Kohn–Sham equations are solved by applying the full potential linearized augmented plane wave (FP-LAPW) method. The exchange correlation effects are included through the local density approximation (LDA), generalized gradient approximation (GGA) and modified Becke–Johnson (mBJ) exchange potential. The calculated lattice constant is in good agreement with the experimental result. The calculation of band structure and density of states shows that these compounds have indirect energy band gap (M–Γ) with a mixed ionic and covalent bonding. Calculations of the optical spectra, viz., the real and imaginary parts of dielectric function, optical reflectivity, photoconductivity and refractive index are performed.

**Keywords:** Optical properties, Band gap, FP-LAPW, Perovskites

## 1. Introduction

Perovskite ( $\text{ABX}_3$ ) is one of the most frequently encountered structures in solid-state physics, and it accommodates most of the metallic ions in the periodic table with a significant number of different anions. However, there are very few studies that have focused on the evolution of the bonding mechanism of ferroelectric perovskite materials according to the lattice distortions. Among the perovskite oxides studied most intensively are zirconates of alkaline earth metals. Indeed, they are currently gaining considerable importance in the field of electrical ceramics, refractories, geophysics, astrophysics, particle accelerators, fission, fusion reactors, heterogeneous catalysis etc. Additionally, they have received great attention as high temperature proton conductors with the possibility of applications in fuel cells or hydrogen sensors [1,2].

Although majority of the perovskite compounds are oxides or fluorides, other forms like heavier halides, sulphides, hydrides, cyanides, oxyfluorides and oxynitrides are also reported [3-5]. Oxide perovskites are popular in major industrial applications due to their diverse physical properties [5] over a wide temperature range. Above the Curie temperature, most of them have ideal cubic crystal structure. As the temperature is lowered, they transform from the high-symmetry para electric phase to slightly distorted ferroelectric structures with tetragonal, orthorhombic and rhombohedral symmetries. Typically, the phase transitions are characterized by a small macroscopic lattice strain and microscopic displacement of ions [6-10]. A large number of the perovskites undergo a series of the structural phase transitions ranging from nonpolar antiferrodistortive to ferroelectric to antiferroelectric in nature as temperature is reduced. These transitions are an outcome of the delicate balance between long-range dipole–dipole interactions that favor the ferroelectric state and

short-range forces that favor the cubic perovskite phase [11]. These structural phase transitions involve very small atomic displacements away from the ideal cubic structure and the energy differences are small. First principles density functional calculations have significant success in providing accurate total-energy surfaces for the perovskites to explain the ferroelectric distortions [8,12]. In our knowledge, neither experimental nor theoretical efforts have been made to explore optoelectronic properties of these ternary oxides. With this motivation, we perform density functional theory (DFT) calculations to probe structural and optoelectronic properties of  $\text{CsCaCl}_3$  and  $\text{KCdF}_3$  cubic perovskites.

## 2. Computational Details

The First-principles calculations were done using FP-LAPW computational scheme [13,14] as implemented in the WIEN2K code [15]. The FP-LAPW method expands the Kohn-Sham orbitals in atomic like orbitals inside the muffin-tin (MT) atomic spheres and plane waves in the interstitial region. The Kohn-Sham equations were solved using the recently developed Wu-Cohen generalized gradient approximation (WC-GGA) [16, 17] for the exchange-correlation (XC) potential. It has been shown that this new functional is more accurate for solids than any existing GGA and meta-GGA forms. For a different type of materials, it improves the equilibrium lattice constants and bulk moduli significantly over local-density approximation [18] and Perdew-Burke-Ernzerhof (PBE) [19] and therefore is a better choice. For this reason, we tried the new WC approximation for the XC potential in studying the present systems. Further for electronic structure calculations modified Becke–Johnson potential (mBJ) [20] as coupled with WC-GGA is used.

The valence wave functions inside the atomic spheres were expanded up to  $l=10$  partial waves. In the interstitial region,

Volume 6 Issue 4, April 2017

[www.ijsr.net](http://www.ijsr.net)

Licensed Under Creative Commons Attribution CC BY

a plane wave expansion with  $R_{MT}K_{max} = 7$  was used for all the investigated systems, where  $R_{MT}$  is the minimum radius of the muffin-tin spheres and  $K_{max}$  gives the magnitude of the largest K vector in the plane wave expansion. The potential and the charge density were Fourier expanded up to  $G_{max} = 12$ . We carried out convergence tests for the charge-density Fourier expansion using higher  $G_{max}$  values. The modified tetrahedron method [20] was applied to integrate inside the Brillouin zone (BZ) with a dense mesh of 5000 uniformly distributed k-points (equivalent to 405 in irreducible BZ) where the total energy converges to less than  $10^{-6}$  Ry.

### 3. Results and Discussion

#### 3.1 Structural properties

$ABX_3$  ( $A = K$ ;  $B = Cd$ ;  $X = F$ ) crystallize in cubic structure having space group Pm-3m (No.221). The A, B and X atoms are positioned at (0 0 0), (1/2, 1/2,1/2), (1/2, 1/2, 0) sites of Wyckoff coordinates respectively. Energy versus volume minimization process [21] is used to calculate equilibrium lattice parameters such as lattice constants ( $a_0$ ), ground state energy ( $E_0$ ), bulk modulus (B), and its pressure derivative ( $B'$ ) by LDA and GGA exchange correlation schemes as shown in Table (1).

**Table 1:** Structural parameters, lattice constants a (Å), ground state energies  $E_0$  (Ry) bulk modulus B (GPa) and its pressure derivative  $B'$  (GPa) with experimental and other theoretical values of  $CsCaCl_3$  and  $KCdF_3$  cubic perovskites.

Structural analysis	a (Å)	a (Å) exp. [1]	$E_0$ (Ry)	$B'$	B (GPa)	B (GPa) [1]
KCdF <sub>3</sub>	4.39 (GGA),	4.29	-12987.502 (GGA), -12980.052 (LDA)	4.27 (GGA), 5.27 (LDA)	66 (GGA), 74 (LDA)	63
	4.31 (LDA)					

In addition to it, we use lattice parameters calculated by generalized gradient approximation (GGA) for investigating electronic and optical properties.

We can also provide a prediction of the bulk modulus by using the semi-empirical equation developed by Verma et al [1]

$$B \text{ (GPa)} = S + V \frac{(Z_a Z_b Z_c)^{0.35}}{a^{3.5}} \quad (1)$$

where  $Z_a$ ,  $Z_b$  and  $Z_c$  are the ionic charges on the A, B and X, respectively and a is lattice parameter in Å. The S and V are constants and the values are 1.79 and 5505.785 respectively.

#### 3.2 Electronic Properties

The electronic properties of herein investigated perovskites are based on energy band structure and total as well as partial density of states (TDOS and PDOS) while influence of bonding nature is discussed in terms of charge density distribution. Graphically, we have highlight recently improved Trans-Blaha modified Becke–Johnson (TB-mBJ) potential, which removes wrong interpretation of the true unoccupied states of the system which causes underestimation of electronic band gap [22]. The calculated band structures of  $KCdF_3$  are shown in fig. 1.

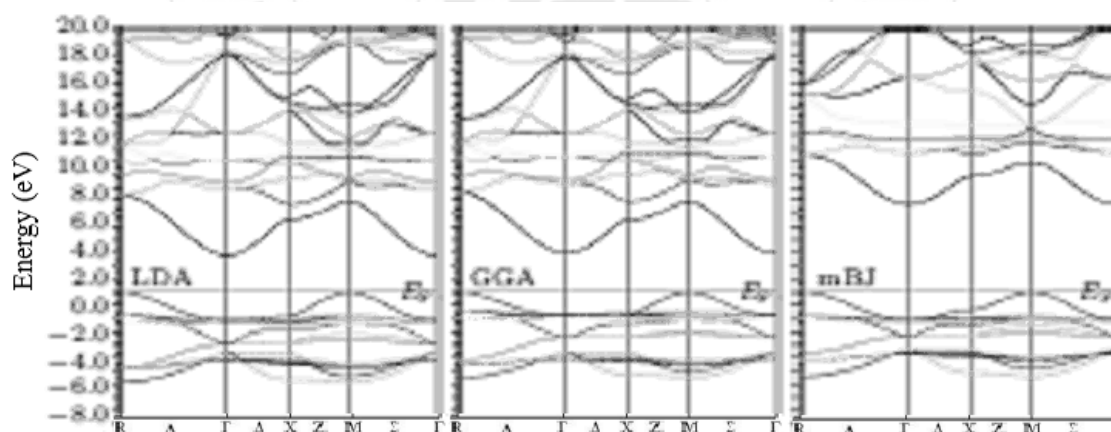


**Figure 1:** Band Structure of  $KCdF_3$

The calculated values of the band gaps for  $KCdF_3$  are found to be equal to 2.99 eV, 3.08 eV, and 6.85 eV by using LDA, GGA and mBJ, respectively. It is observed that overall trend of band dispersion curves are almost same but conduction band minimum (CBM) lies at  $\Gamma$  and valence band maximum (VBM) lies at M symmetry point of Brillouin zone (BZ) revealing (M- $\Gamma$ ) indirect band gap of 6.85 eV for  $KCdF_3$  compound.

On the basis of different bands; the total density of states (TDOS) could be grouped into four regions and the contribution of different states in these bands can be seen

from the partial density of states (PDOS). From Figure. 2(b) for  $KCdF_3$ , it is seen that the TDOS of the compound can be grouped into different regions within energy range  $-7$  eV to 20 eV. The narrow band around  $-5$  eV is due to Cd 4d states contribution observed. From  $-3$  eV to the Fermi level, the bands have major contribution of F 2p states and minor contribution of Cd 4d states. There is hybridization between Cd 4d with F 2p states in this region. Above the Fermi level, the conduction band minimum (CBM) is composed by Cd 5s states. From 10 eV to 14 eV, majority contribution is due to K 3d states. The occupied states correspond to the valence band, where the unoccupied states are related to the

conduction band. In the present case the K 3p states are occupied and K 3d states are unoccupied. Therefore, the majority contribution comes from K 3d states rather than K 3p states in the conduction band. From 14 eV to 20 eV, along with K 3d states a minor contribution of Cd 4f states is observed. These calculations have been measured theoretically and experimentally for KCdF<sub>3</sub> by Babu et al. [23, 24] and Macdonald et al [25] respectively. Our theoretical calculations are in good agreement with their results.

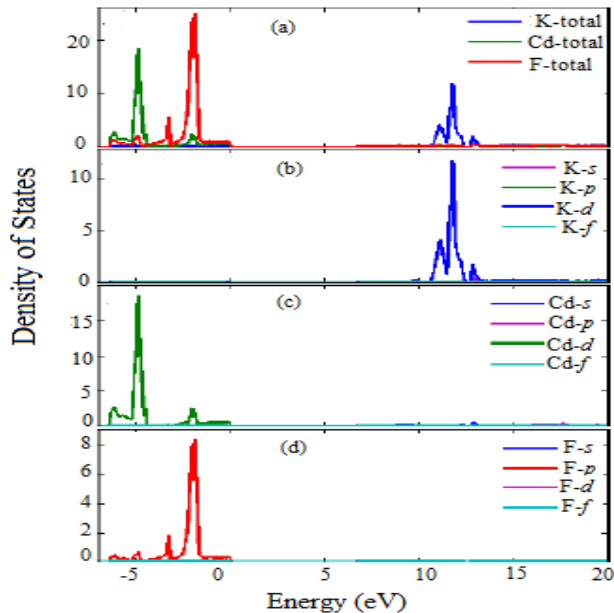


**Figure 2:**Total Density of States of KCdF<sub>3</sub>.

### 3.3 Optical properties

The linear response to an external electromagnetic field with a small wave vector is measured through the complex dielectric function,

$$\epsilon(\omega) = \epsilon_1(\omega) + i\epsilon_2(\omega) \quad (2)$$

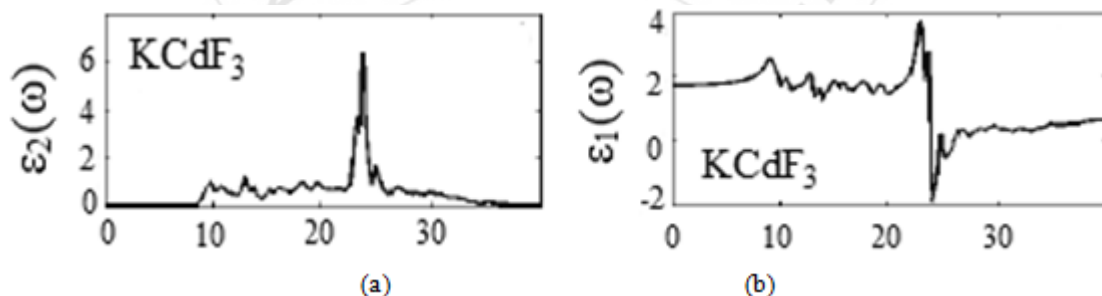


**Figure 3:** The calculated (a) imaginary  $\epsilon_2(\omega)$  and (b) real  $\epsilon_1(\omega)$  parts of complex dielectric constant of KCdF<sub>3</sub> perovskites.

The refractive index is displayed in fig. 4a for KCdF<sub>3</sub> respectively, we observe the optically isotropic nature of this compound in the lower energy range. For lower energies the refractive index value is almost constant and as the energy increases it attains a maximum value and exhibits decreasing tendency for higher energy values. The static refractive index  $n(0)$  for KCdF<sub>3</sub> is found to have the value 1.28. The refractive index is greater than one because as photons enter a material they are slowed down by the interaction with

which is related to the interaction of photons with electrons [26]. The imaginary part  $\epsilon_2(\omega)$  of the dielectric function could be obtained from the momentum matrix elements between the occupied and unoccupied wave functions and is given by [27]

$$\epsilon_2(\omega) = \frac{4\pi^2 e^2}{m^2 \omega^2} \sum_j \langle i | M | j \rangle^2 f_i (1 - f_j) \times \delta[E_j - E_i - \omega] d^3k. \quad (3)$$

The real part  $\epsilon_1(\omega)$  can be evaluated from  $\epsilon_2(\omega)$  using the Kramer-Kronig relations and is given by [28]

$$\epsilon_1(\omega) = 1 + \left( \frac{2}{\pi} \right) \int_0^\infty \frac{\omega' \epsilon_2(\omega')}{\omega'^2 - \omega^2} d\omega'. \quad (4)$$

All of the other optical properties, including the photoconductivity ( $\sigma(\omega)$ ) refractive index (n) and reflectivity (R( $\omega$ )) can be directly calculated from  $\epsilon_1(\omega)$  and  $\epsilon_2(\omega)$  [26,28].

The imaginary part  $\epsilon_2(\omega)$  and the real part  $\epsilon_1(\omega)$  of the dielectric function, refractive index (n), reflectivity (R( $\omega$ )), and photoconductivity ( $\sigma(\omega)$ ) of KCdF<sub>3</sub> are shown in fig. 3 and 4, as functions of the photon energy in the range of 0-30 eV. The imaginary part  $\epsilon_2(\omega)$  of KCdF<sub>3</sub> in fig. 3 (a) the threshold energy of the dielectric function occurs at E = 8.27 eV respectively, which corresponds to the fundamental gap at equilibrium. It is well known that the materials with band gaps larger than 3.1 eV work well for applications in the ultraviolet (UV) region of the spectrum [29]. Hence this wide band gap material could be suitable for the high frequency UV device applications. The real part of the dielectric function  $\epsilon_1(\omega)$  is displayed in fig. 3b for KCdF<sub>3</sub>. This function  $\epsilon_1(\omega)$  gives us information about the electronic polarizability of a material. The static dielectric constant at zero is obtained as  $\epsilon_1(0) = 1.69$  for KCdF<sub>3</sub> which is approximately same as calculated by Nurullah et al [30].

electrons. The more photons are slowed down while traveling through a material, the greater the material's refractive index. Generally, any mechanism that increases electron density in a material also increases refractive index. The photoconductivity ( $\sigma(\omega)$ ) is shown in fig. 4b for KCdF<sub>3</sub> respectively. It starts from 6.93 eV for and 8.61 eV for KCdF<sub>3</sub> the maximum value of optical

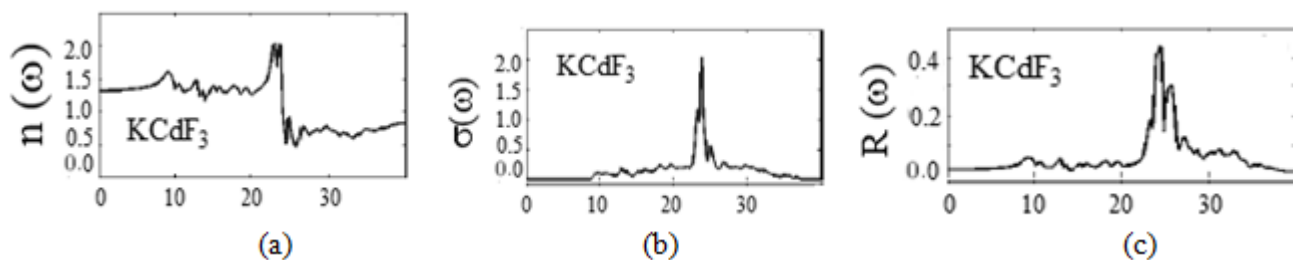


**Figure 4:** The calculated (a) refractive index ( $n(\omega)$ ), (b) photoconductivity ( $\sigma(\omega)$ ) and (c) reflectivity ( $R(\omega)$ ) of  $\text{KCdF}_3$  perovskites

conductivity of the  $\text{KCdF}_3$  is obtained at 23.85 eV. The reflectivity ( $R(\omega)$ ) for  $\text{KCdF}_3$  is shown in fig. 4c. The zero-frequency reflectivity ( $R(\omega)$ ) is 1.71% for  $\text{KCdF}_3$  which remains almost the same up to 19.5 eV for  $\text{KCdF}_3$ . The maximum reflectivity ( $R(\omega)$ ) value is about 43.15%, which occurs at 24.30 eV for  $\text{KCdF}_3$ .

#### 4. Conclusions

In this paper, We have presented a theoretical analysis of the structural and optoelectronic properties of ternary oxides using FP-LAPW method within LDA, GGA approximation and mBJ potential. The use of CGA for the exchange-correlation potential permitted us to obtain good structural properties. Detailed analysis of electronic properties authenticates that  $\text{CsCaCl}_3$  and  $\text{KCdF}_3$  are indirect band gap semiconductors (M- $\Gamma$ ) with mixed nature of ionic and covalent bonding. Finally, the optical properties such as complex dielectric function  $\epsilon(\omega)$ , optical conductivity  $\sigma(\omega)$ , refractive index  $n(\omega)$  and reflectivity  $R(\omega)$  are studied. The prominent value of static dielectric constant of herein studied material suggests that  $\text{KCdF}_3$  can play a significant role in miniaturization technology.

#### 5. Acknowledgment

The first author (Madan Lal) wishes to thank I. K. Gujral Punjab Technical University (PTU), Jalandhar for helping and providing the facilities.

#### References

- [1] A. S. Verma and A. Kumar,.; Bulk modulus of cubic perovskites, *J. Alloys and Compounds*, 541, pp.210-214,2012.
- [2] A. S. Verma and V. K. Jindal, lattice constants of cubic perovskite, *J. Alloys and Compounds*, 485(1-2), pp.514-518,2009.
- [3] A. S. Verma, Elastic moduli of orthorhombic perovskites, *Solid State Communications*, 158, p.p.34-37,2013.
- [4] A. S. Verma, A. Kumar and S. R. Bhardwaj; Correlation between ionic charge and the lattice constant of cubic perovskite solids *Physica Status Solidi B*, 245(8), pp.1520-1526,2008.
- [5] M. W. Lufaso and P.M. Woodward, Predictions of the Crystal Structures of Perovskites Using the Software Program SpuDS, *Acta Cryst. B*, 57, pp.725-738,2001.
- [6] H. Iwahara, M. Balkanski, T. Takahashi and H.L. Tuller (Eds.), *Solid State Ionics*, Elsevier, Amsterdam,1992.
- [7] T. Mori, K. Aoki, N. Kamegashira and T. Shishido, Crystal structure of  $\text{DyMnO}_3$ , *Mater. Lett.* 42, pp.387-389,2000.
- [8] R. D. King-Smith and D. Vanderbilt, First-principles investigation of ferroelectricity in perovskite compounds, *Phys. Rev. B*, 49, pp.5828-5844,1994.
- [9] R. E. Cohen and H. Krakauer, Lattice dynamics and origin of ferroelectricity in  $\text{BaTiO}_3$ : Linearized-augmented-plane-wave total-energy calculations, *Phys. Rev. B* 42(10), pp.6416-6423,1990.
- [10] W. D. Xue et al., First-principles study on tetragonal  $\text{BaTiO}_3$  ferroelectric, *Acta Phys. Sin.* 54(2), pp.857-862,2005.
- [11] M. E. Lines and A. Glass, *Principles and Applications of Ferroelectric and Related Materials*, Clarendon Press, Oxford, 1977.
- [12] R. D. King-Smith and D. Vanderbilt, A first-principles pseudopotential investigation of ferroelectricity in barium titanate, *Ferroelectrics*, 136, pp.85-94,1992.
- [13] G. K. H. Madsen, P. Blaha, K. Schwarz, E. Sjöstedt, L. Nordström, Efficient linearization of the augmented plane-wave method, *Phys. Rev. B* 64, 195134,2001.
- [14] K. Schwarz, P. Blaha, G. K. H. Madsen, Electronic structure calculations of solids using the WIEN2K package, *Comput. Phys. Commun.* 147, 71,2002.
- [15] P. Blaha, K. Schwarz, G. K. H. Madsen, D. Kvasnicka, J. Luitz: WIEN2k: An Augmented Plane Wave+Local Orbitals Program for Calculating Crystal Properties' (Karlheinz Schwarz/Techn. Universität Wien, Austria,2001.
- [16] Z. Wu, R. E. Cohen, *Phys. Rev. B*, More accurate generalized gradient approximation for solids, 73, 235116,2006.
- [17] F. Tran, R. Laskowski, P. Blaha, K. Schwarz, Performance on molecules, surfaces, and solids of the Wu-Cohen GGA exchange-correlation energy functional, *Phys. Rev. B* 75, 115131,2007.
- [18] W. Kohn, L. J. Sham, "Self-Consistent Equations Including Exchange and Correlation Effects" *Phys. Rev.* No. 140, A1133,1965.
- [19] J. P. Perdew, K. Burke, M. Ernzerhof, Generalized Gradient Approximation Made Simple, *Phys. Rev. Lett.* 77(18), 3865,1996.
- [20] F. Tran, P. Blaha, Accurate Band Gaps of Semiconductors and Insulators with a Semilocal Exchange-Correlation Potential, *Phys. Rev. Lett.* Vol.102(22), 226401,2009.
- [21] F. D. Murnaghan, *Proc. Natl. Acad. Sci. USA* vol. 30(9), pp.244-247,1994.

- [22] H.C. Kandpal, G.H. Fecher, C. Felser, Calculated electronic and magnetic properties of the half-metallic, transition metal based Heusler compounds, J. Phys. D. Vol. 40(6) pp.1507-1523,2007.
- [23] K. E. Babu, N. Murali, K. V. Babu, P. T. Shibeshi and V. Veeraiah, Structural, Elastic, Electronic, and Optical Properties of Cubic Perovskite CsCaCl<sub>3</sub> Compound: An ab initio Study, Acta Physica Polonica A 125, pp.1179-1185,2014.
- [24] K. E. Babu, N. Murali, K. V. Babu, B. K. Babu and V. Veeraiah, Elastic and Optoelectronic Properties of KCdF<sub>3</sub>: ab initio Calculations through LDA/GGA/TB-mBJ within FP-LAPW Method, Chin. Phys. Letts. 32, 016201,2015
- [25] M.A. Macdonald, E.N. Melchakov, I.H. Munro, P.A. Rodnyi, A.S. Voloshinovskiy, Radiative core-valence transitions in CsMgCl<sub>3</sub> and CsSrCl<sub>3</sub>, J. Lumin. 65, pp.19-23,1995.
- [26] M. Q. Cai, Z. Yin, M. S. Zhang, First-principles study of optical properties of barium titanate Appl. Phys. Letts 83, 2805,2003.
- [27] M. Catti, Acta Crystallogr. Crystal elasticity and inner strain: a computational model A 45, pp.20-25,1989.
- [28] S. Saha, T. P. Sinha, A. Mookerjee, Electronic structure, chemical bonding, and optical properties of paraelectric BaTiO<sub>3</sub>, Phys. Rev. B 62, 8828,2000.
- [29] M. Maqbool, B. Amin, I. Ahmad, Bandgap investigations and the effect of the In and Al concentration on the optical properties of In<sub>x</sub>Al<sub>1-x</sub>N In<sub>x</sub>Al<sub>1-x</sub>N J. Opt. Soc. Am. B 26, pp. 2181-2184,2009.
- [30] M. Nurullah Secuk, Emel Kilit Dogan, Murat Aycibin, Bahattin Erdinc and Harun Akkus, Investigation of structural, electronic and optical properties of KCdF<sub>3</sub>, American Journal of Modern Physics, 2(2), pp.77-80,2013.